Engineered Zinc Finger Protein–Mediated VEGF-A Activation Restores Deficient VEGF-A in Sensory Neurons in Experimental Diabetes

Elizabeth J. Pawson,[1] Beatriz Duran-Jimenez,[1] Richard Surosky,[2] Heather E. Brooke,[1] S. Kaye Spratt,[2] David R. Tomlinson,[1] and Natalie J. Gardiner[1]

OBJECTIVE—The objectives of the study were to evaluate retrograde axonal transport of vascular endothelial growth factor A (VEGF-A) protein to sensory neurons after intramuscular administration of an engineered zinc finger protein activator of endogenous VEGF-A (VZ+434) in an experimental model of diabetes, and to characterize the VEGF-A target neurons.

RESEARCH DESIGN AND METHODS—We compared the expression of VEGF-A in lumbar (L)4/5 dorsal root ganglia (DRG) of control rats and VZ+434-treated and untreated streptozotocin (STZ)-induced diabetic rats. In addition, axonal transport of VEGF-A, activation of signal transduction pathways in the DRG, and mechanical sensitivity were assessed.

RESULTS—VEGF-A immunoreactivity (IR) was detected in small- to medium-diameter neurons in DRG of control rats. Fewer VEGF-A-IR neurons were observed in DRG from STZ-induced diabetic rats; this decrease was confirmed and quantified by Western blotting. VZ+434 administration resulted in a significant increase in VEGF-A protein expression in ipsilateral DRG, 24 h after injection. VEGF-A was axonally transported to the DRG via the sciatic nerve. VZ+434 administration resulted in significant activation of AKT in the ipsilateral DRG by 48 h that was sustained for 1 week after injection. VZ+434 protected against mechanical allodynia 8 weeks after STZ injection.

CONCLUSIONS—Intramuscular administration of VZ+434 increases VEGF-A protein levels in L4/5 DRG, correcting the deficit observed after induction of diabetes, and protects against mechanical allodynia. Elevated VEGF-A levels result from retrograde axonal transport and are associated with altered signal transduction, via the phosphatidylinositol 3′-kinase pathway. These data support a neuroprotective role for VEGF-A in the therapeutic actions of VZ+434 and suggest a mechanism by which VEGF-A exerts this activity. ***Diabetes*** **59:509–518, 2010**

The vascular endothelial growth factor (VEGF) family consists of seven secreted glycoproteins, named VEGF-A to -F and placental growth factor. The prototypic VEGF family member, VEGF-A, was first demonstrated to enhance vascular permeability and promote the proliferation, migration, and survival of endothelial cells leading to increased angiogenesis and tissue perfusion (1). In addition to its angiogenic properties, both neurotrophic and neuroprotective functions for VEGF-A have been described in both sensory (2–6) and motor (7) neurons.

The VEGFs bind to, and signal through, specific receptor tyrosine kinases: VEGF receptor (VEGFR)-1 (Flt-1); VEGFR-2 (KDR; Flk-1); and the neuropilin receptors 1 and 2 (8,9), as well as via interaction with heparin sulfate proteoglycans (10). VEGF-A can activate both the mitogen-activated protein kinases (MAPKs) and the phosphatidylinositol 3′-kinase (PI3-K) signal transduction pathways (11), and both of these pathways have been implicated as mediators of the phenotypic abnormalities observed in sensory neurons during the development of diabetic neuropathy (12–15).

VEGF-A mRNA is alternatively spliced to express three major protein isoforms, VEGF-A_{121}, VEGF-A_{165}, and VEGF-A_{189}. Both experimental and clinical studies have indicated improvements in the signs and symptoms of sensory diabetic neuropathy after intramuscular injection of a plasmid DNA encoding a single isoform of VEGF-A, $VEGF_{165}$-A (16–18). However, several preclinical studies suggest that the combination of all three VEGF-A isoforms may provide more potent biological activity (19–21). Given the importance of all VEGF-A isoforms, we have chosen to investigate an alternative strategy for the therapeutic application of this growth factor, namely, the activation of the endogenous VEGF-A gene through the action of an engineered zinc finger protein–transcription factor (ZFP-TF). Transfection of plasmid DNA encoding the VEGF-A–activating ZFP-TF, VZ+434, results in the expression of all three major isoforms of VEGF-A in their correct proportions (22). Moreover, it has also been demonstrated that intramuscular administration of VZ+434 drives therapeutic angiogenesis (23) and provides significant, and dose-related, protection of both motor and sensory nerve conduction velocity (NCV) deficits in streptozotocin (STZ)-induced diabetic rats (24). ZFP-TF–driven VEGF-A activation thus has both neuroprotective and angiogenic effects that could contribute directly (or indirectly) to improvements in NCV.

To begin to investigate the mechanism(s) by which VEGF-A affects nerve function, we have examined retrograde axonal transport of VEGF-A protein after intramuscular administration of VZ+434 in the rat STZ-induced model of diabetic neuropathy. We show that VEGF-A is normally expressed in small- to medium-diameter sensory neurons of the dorsal root ganglia (DRG), and is downregulated in diabetes. However, VEGF-A protein levels can be normalized by intramuscular injection of VZ+434. Plasmid DNA encoding VZ+434 is found in the muscle but not in the DRG, whereas VEGF-A protein is shown to

From the [1]Faculty of Life Sciences, University of Manchester, Manchester, U.K.; and [2]Sangamo Biosciences, Richmond, California.
Corresponding author: Natalie Jane Gardiner, natalie.gardiner@manchester.ac.uk.
Received 3 November 2008 and accepted 30 October 2009. Published ahead of print at http://diabetes.diabetesjournals.org on 23 November 2009. DOI: 10.2337/db08-1526.
E.J.P. and B.D.-J. contributed equally to this study.

TABLE 1
Blood glucose and body weight measurements

Group no.	Experimental details	Blood glucose (mmol/l)	Body weight (g)	
			Start	End
Experiment 1				
1	Diabetic + VZ + 434 24 h	26.0 ± 1.7	324 ± 6	334 ± 48
2	Diabetic + VZ + 434 48 h	25.9 ± 1.6	280 ± 16	229 ± 18
3	Diabetic + VZ + 434 1 week	20.8 ± 4.2	317 ± 10	335 ± 48
4	Diabetic + VZ + 434 2 weeks	23.3 ± 4.3	326 ± 16	376 ± 78
5	Control	7.9 ± 0.4	332 ± 18	491 ± 5
Experiment 2				
1	Diabetic + VZ + 434 24 h	19.1 ± 2	274 ± 14	257 ± 20
2	Diabetic + VZ + 434 + sciatic ligature 24 h	21.1 ± 2.1	287 ± 24	271 ± 25
3	Diabetic + ligature 24 h	18.5 ± 2.3	278 ± 15	247 ± 13
4	Diabetic untreated	22.6 ± 5.7	280 ± 16	270 ± 28
5	Control untreated	8 ± 1.4	272 ± 16	352 ± 26

Data are means ± SD (n = 4 per group). Two studies were performed in STZ-induced diabetic rats: experiment 1, time course study; and experiment 2, axonal transport study. Final blood glucose levels and start and end body weights for all groups are shown.

undergo axonal transport to the DRG, 24 h after VZ+434. In addition, we demonstrate sustained activation of AKT in the DRG, demonstrating a functional consequence to the increased VEGF-A levels in this tissue, which may underlie the neuroprotective effect of VZ+434-mediated VEGF-A activation in STZ-induced diabetic rats.

RESEARCH DESIGN AND METHODS

Induction of diabetes. All studies and procedures were licensed under the U.K. Animals (Scientific Procedures) Act 1986. Diabetes was induced in adult male Wistar rats (250–300 g; Charles River, Margate, U.K.) via intraperitoneal injection of freshly dissolved STZ (55 mg/kg in sterile saline), administered after an overnight fast. Diabetes was verified 3 days after STZ injection using a strip-operated reflectance photometer (OptimumPlus; MediSense, Whitney, U.K.) to measure the animal's tail vein blood glucose levels. Rats with blood glucose less than 15 mmol/l were excluded from the study. Age- and weight-matched rats were used as nondiabetic controls. The VEGF-A activating ZFP-TF VZ+434 has previously been described (22). Plasmids were formulated at a concentration of 2 mg/ml in 5% poloxamer 188 (BASF, Florham, NJ), 150 mmol/l NaCl, and 2 mmol/l Tris (pH 8.0; Sangamo BioSciences).

Study design. Three weeks after induction of diabetes, control and STZ-induced diabetic rats were anesthetized with isoflurane (2% in oxygen) and were either injected with a total of 250 μg VZ+434 at two sites in their left gastrocnemius/soleus muscle, or left untreated.

After injection of VZ+434, additional groups of treated and untreated diabetic rats also had their left sciatic nerve exposed and ligated with polypropylene monofilament nonabsorbable sutures (Prolene; Ethicon) at mid-thigh level, proximal to the site of injection. The wound was closed and animals recovered under observation. Rats were killed at selected time points after injection with VZ+434 (1, 2, 7, and 14 days), or for the sciatic nerve ligation studies at 1 day after ligation.

Ipsilateral and contralateral muscle, sciatic nerves, and lumbar (L)4/5 DRG were removed. Tissue designated for Western blot analysis was snap frozen in liquid nitrogen and stored at −40°C until processing. Sciatic nerve and DRG samples destined for immunohistochemical studies were postfixed in 4% paraformaldehyde overnight at 4°C, then cryoprotected in 30% sucrose in 0.1 M phosphate buffer for 24 h at 4°C. Tissues were then frozen in OCT embedding medium (VWR, Lutterworth, U.K.) and stored at −40°C until processing.

For sensory testing experiments, STZ-induced diabetic rats were either untreated or treated with 250 μg VZ+434 at 4, 6, and 8 weeks after STZ injection, in two sites in their left gastrocnemius/soleus muscle (n = 6–10 per group). Behavioral responses of STZ-induced diabetic rats and age-matched control rats to tactile stimulation were measured at baseline (before STZ injection), and at 4, 8, and 12 weeks after STZ injection.

Western blotting. Western blotting was conducted as previously described (25). Blots were incubated overnight at 4°C with primary antibodies: anti–VEGF-A (1:500; Santa Cruz Biotechnology), anti–total extracellular signal–related kinase (ERK; 1:2000; Cell Signaling Technology, Danvers, MA), anti–phospho AKT and anti–total AKT (1:2000; Cell Signaling Technology), and anti–βIII-tubulin (1:1,000; Sigma). Blots were washed and incubated in horseradish peroxidase–linked anti-rabbit IgG or anti-mouse IgG (1:2000; Cell Signaling Technology) for 1 h at room temperature. Protein bands were visualized using LumiGLO and Peroxidase Reagent (Cell Signaling Technology). The films were scanned, and the total pixel intensity for each band was calculated using SigmaScan Pro5 software (SPSS, Chicago, IL). Graphs and statistical analyses were prepared using GraphPad PRISM 4 software. Data were analyzed using either one-way ANOVA followed by either the Dunnett post hoc test, Student paired t test, or Student one-sample t test as appropriate. Data are expressed as mean ± SD.

Immunohistochemistry. Longitudinal sections (12-μm) of sciatic nerve or L4/5 DRG were thaw-mounted onto Superfrost Plus Slides (VWR). Sections were washed with PBS, and then incubated in blocking buffer (10% normal donkey serum, 0.2% Triton-X_{100} in PBS) for 1 h at room temperature. Slides were incubated overnight at either 4°C or room temperature with primary antibodies (in blocking buffer): anti–VEGF-A (1:500; Santa Cruz Biotechnology), anti–calcitonin gene-related peptide (CGRP; 1:500; Sigma), anti–neurofilament 200 (NF200; 1:400; Chemicon), anti-S100β (1:500; Sigma), or anti–phospho (p) AKT (1:100; Promega). Slides were washed and then incubated with either cyanin 3–conjugated donkey anti-rabbit and/or fluorescein isothiocyanate–conjugated donkey anti-mouse IgG as appropriate (1:200; Jackson ImmunoResearch) for 1 h at room temperature. In addition some slides were colabeled with fluorescein isothiocyanate–conjugated isolectin B4 from *Griffonia simplicifolia* (20 μg/ml; Vector Labs, Peterborough, U.K.). Sections were mounted in Vectorshield containing DAPI (Vector Labs). Immunofluorescence was visualized using a Leica MPS60 DMR fluorescent microscope. Digital images were acquired using WASABI software (Hamamatsu Photonics, Herts, U.K.) and processed using Adobe Photoshop CS (Adobe Systems).

Image analysis. The threshold for high VEGF-A immunoreactivity (IR) was determined by calculating the mean staining intensity of four neurons per animal that were deemed to be positively stained (SigmaScan Pro). This mean intensity was then taken as the threshold value to determine the percentage of VEGF-A-IR neuronal profiles. All neuronal profiles were traced and mean VEGF-A-IR and Feret diameter of each profile were automatically calculated (SigmaScan Pro) and data were used for cell size distribution analysis. Cell profiles from four randomly selected sections (each 100-μm apart) of ipsilateral and contralateral L4/5 DRG (processed on the same slide) from four animals in each treatment group were measured. The method of recursive translation was applied to these results to correct for overestimation of both large and small-diameter cell profiles (26).

Taqman and quantitative RT-PCR. VZ+434 plasmid DNA levels were measured in duplicate reactions containing 100 ng of DNA and TaqMan Universal PCR Mix (Applied Biosystems, Foster City, CA). Reactions were analyzed using an ABI 7300 Real Time PCR System (Applied Biosystems). Plasmid copy numbers (PCNs) were determined from a standard curve prepared from a 10-fold serial dilution of VZ+434. The background PCN level was determined from the mean of VZ+434 levels in tissues from the right (contralateral) side plus 2 SD.

Testing of mechanical thresholds. At 1 week prior to, and at 4, 8, and 12 weeks after induction of diabetes, the behavioral response to mechanical stimulation of the hind paw was assessed using a dynamic plantar aesthesiometer (Ugo Basile, Comerio, Italy). Paw withdrawal responses were measured in both right and left hind paws in all animals, and are reported as the mean of three measurements per paw, taken at least 10 min apart. Testing was

repeated over two consecutive days, with results recorded from the second day of testing. The assessor was blinded to the VZ+434-treated and untreated STZ groups.

RESULTS

VEGF-A is downregulated in the DRG of STZ-induced diabetic rats compared with control rats. Using Western blot and immunocytochemical analysis, we compared the expression of VEGF-A in L4/5 DRG of control rats and rats 3 weeks after induction of STZ-induced diabetes (see Table 1 for details of blood glucose levels and body weight). VEGF-A levels were significantly reduced in L4/5 DRG from rats 3 weeks after STZ injection (control rats: 16.6 ± 3.2 versus diabetic rats: 3.9 ± 1.6 arbitrary units [AU], $P < 0.0001$, Fig. 1*A* and *B*).

VEGF-A-IR was clearly detected within the cytoplasm of a population of small- to medium-diameter sensory neurons in the DRG of control rats (Fig. 1*C*, arrows) and also in motor neurons in the ventral horn of the spinal cord (data not shown). Fewer VEGF-A-IR neurons were observed in DRG from STZ-induced diabetic rats (Fig. 1*D* and *E*, control rats: 6.5 ± 2.7% VEGF-A-IR neurons versus diabetic rat: 1.9 ± 2.2% VEGF-A-IR neurons; $P < 0.01$). Immunofluorescence was abolished by omission of the primary antibody, indicating the VEGF-A-IR to be primary-antibody specific (data not shown).

Intramuscular administration of VZ+434 increases VEGF-A in the ipsilateral DRG of STZ-induced diabetic rats. A single intramuscular dose of the VEGF-A–activating zinc finger protein transcription factor VZ+434 resulted in a rapid and significant increase in VEGF-A protein expression in ipsilateral L4/5 DRG (Fig. 2). This increase was evident as early as 24 h after injection (left: 5.2 ± 1.2 versus right: 1.0 ± 0.2 AU, $P < 0.05$); VEGF-A levels were normalized by 1 week after injection (Fig. 2*A* and *B*). VEGF-A-IR was detected in contralateral (Fig. 2*C*) and ipsilateral (Fig. 2*D*) L4/5 DRG within a population of small- to medium-diameter sensory neurons (Fig. 2*C* and *D*; arrows). Intramuscular treatment with VZ+434 generated a significant increase in VEGF-IR in small-diameter neurons in the ipsilateral compared with contralateral DRG. VEGF-A-IR was significantly elevated in neurons with diameters between 18.75 and 22.5 μm compared with contralateral DRG (Fig. 2*E* and *F*, $P < 0.05$).

To further characterize the population of VEGF-A-IR neurons in ipsilateral L4/5 DRG, we performed dual immunofluorescence experiments with anti–VEGF-A (Fig. 3*A*, *C*, and *E*) and three neurochemical phenotypic markers: CGRP (Fig. 3*B*), to label small-diameter nociceptive peptidergic neurons; isolectin B4 (IB4; Fig. 3*D*), a marker for nonpeptidergic small-diameter sensory neurons; and NF200 (Fig. 3*F*), a heavy chain neurofilament protein that labels predominantly large-diameter proprioceptive and mechanoreceptive sensory neurons. VEGF-A-IR was observed predominantly in the CGRP-IR and IB4-positive populations, whereas very few VEGF-A-IR neurons colocalized with NF200-IR (Fig. 3*E* and *F*).

Plasmid DNA encoding VZ+434 is not transported to, or transcribed within, the DRG. To investigate the mechanism by which intramuscular VZ+434 normalized VEGF levels in the DRG of diabetic rats, we measured VZ+434 DNA in ipsilateral and contralateral muscle and L4/5 DRG samples from diabetic rats, 24 h after a single intramuscular dose of VZ+434 (Fig. 4).

The background PCN of VZ+434 was set at 2,700 (derived from mean plus 2 SD from contralateral tissue

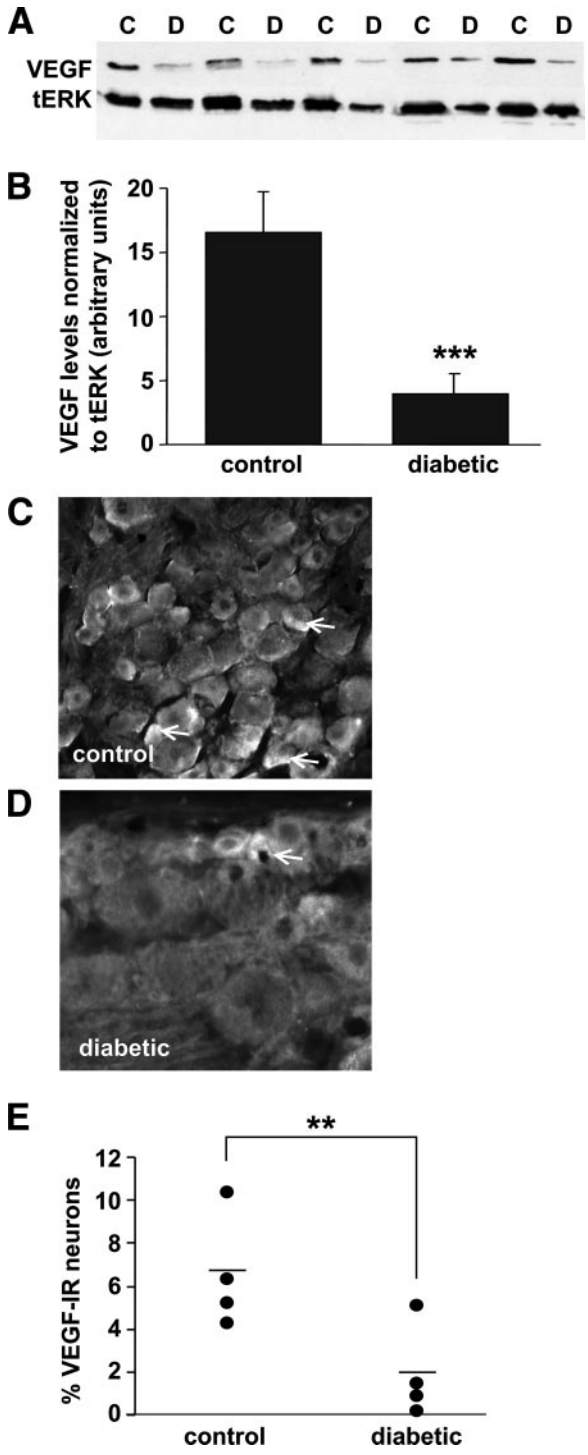

FIG. 1. VEGF-A is downregulated in the DRG of STZ-induced diabetic rats. Western blot analysis of VEGF-A levels in pooled L4/5 DRG obtained from control (C) rats or diabetic rats 3 weeks after STZ injection (D) show a dramatic decrease in VEGF-A in diabetes (*A*). Densitometric analysis of VEGF-A protein levels (normalized to total ERK to correct for protein loading) shows a significant decrease after STZ injection (*$P < 0.0001$, *t* test, $n = 5$ per group, *B*). Representative micrographs show that VEGF-A-IR is present in sensory neurons in L4/5 DRG. A population of small- to medium-diameter neurons in DRG from control rat DRG shows VEGF-A-IR (arrows, *C* and *E*). Fewer VEGF-A-IR neurons were observed in DRG obtained from STZ-induced diabetic rats (*D* and *E*). Data for individual animals ($n = 4$ per group, **$P < 0.01$, *t* test) are shown as circles and the mean value is shown as a horizontal bar (*E*). Scale bar, 50 μm.**

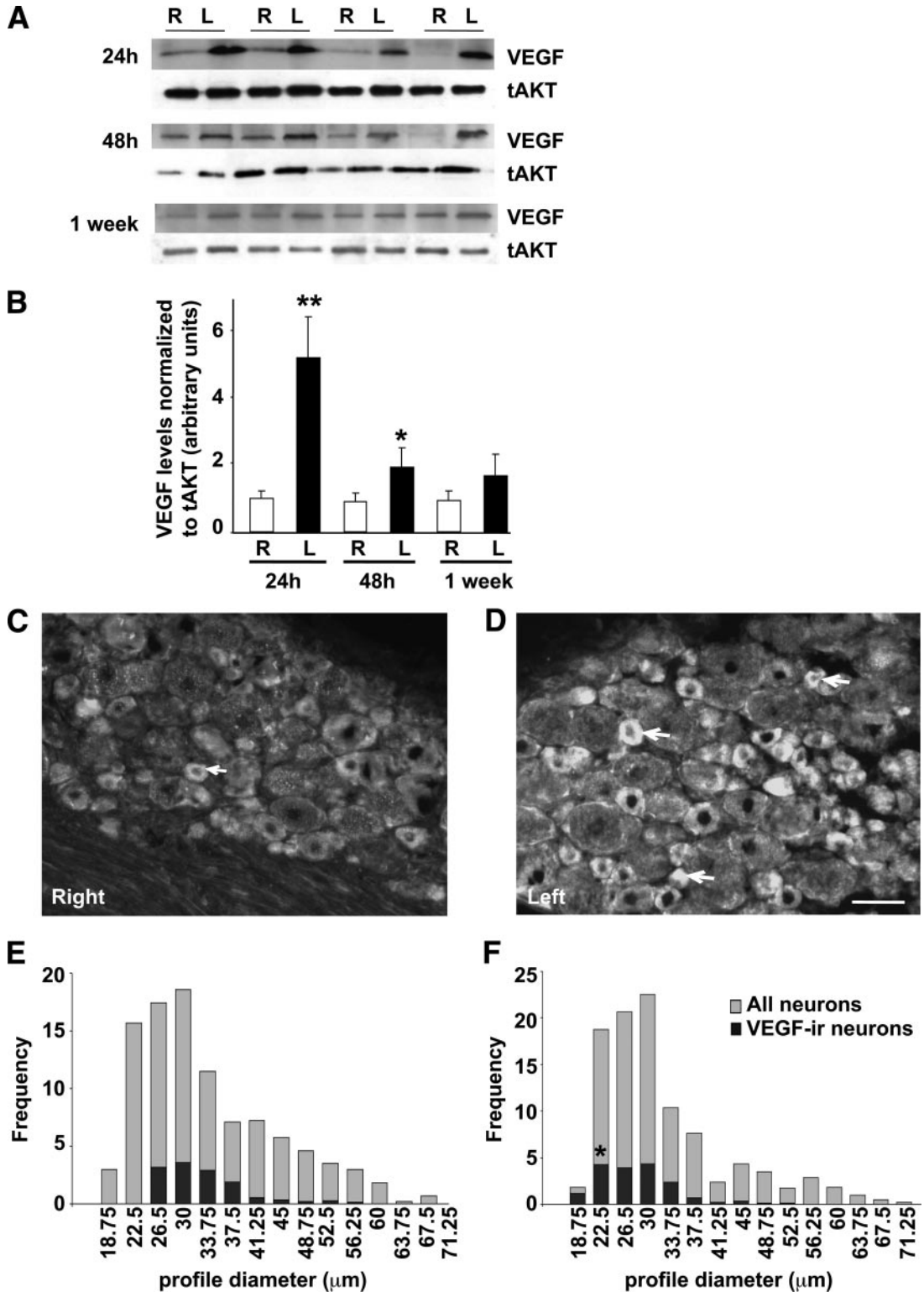

FIG. 2. Intramuscular administration of VZ+434 increases VEGF-A in the ipsilateral DRG of STZ-induced diabetic rats. Diabetic rats (3 weeks after STZ injection) received two intramuscular injections of the VEGF-A–activating zinc finger protein-transcription factor VZ+434 (250 μg total) into the gastrocnemius muscle and were killed at the indicated time points after injection ($n = 4$ per time point). VEGF-A levels in right (uninjected, contralateral limb) and left (injected, ipsilateral limb) were assessed using Western blotting (*A*) and quantified using densitometry (normalized to total AKT to correct for protein loading; *B*). Intramuscular VZ+434 caused a rapid and significant increase in VEGF-A protein expression in ipsilateral L4/5 DRG compared with contralateral by 24 h after injection (*A* and *B*, *$P < 0.05$, **$P < 0.01$ paired t test). Increased VEGF-A-IR (*C* and *D*, arrows) was clearly detected within a population of small- to medium-diameter sensory neurons in the ipsilateral DRG (left, *D*) compared with the contralateral DRG (right, *C*). Cell size distribution analysis shows a significant increase in VEGF-A-IR neurons in small-diameter neurons in the ipsilateral (*F*, *$P < 0.05$, ANOVA) compared with contralateral DRG (*E*). Scale bar, 50 μm.

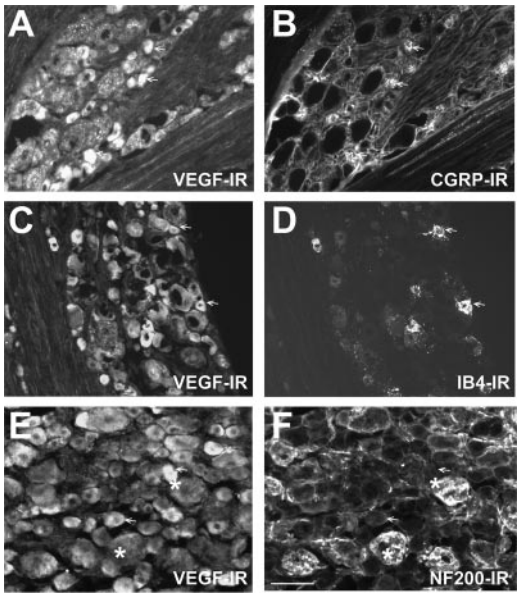

FIG. 3. Phenotypic characterization of VEGF-A-IR neurons in L4/5 DRG of diabetic rats after VZ+434. Representative micrographs show that VEGF-A-IR is present in sensory neurons in L4/5 DRG. Sections have been dual labeled with (*A*, *C*, and *E*) anti–VEGF-A and anti-CGRP (*B*); IB4 (*D*); and anti-NF200 (*F*). A large proportion of neurons that express VEGF-A-IR (*A* and *C*, arrows) coexpress the phenotypic markers CGRP (*B*, arrows) and IB4 (*D*, arrows). Note, very few VEGF-A-IR neurons colocalize with NF200 (*E* and *F*, asterisk). Scale bar, 50 μm.

samples). Ipsilateral muscle contained significantly more copies of VZ+434 than contralateral muscle (mean values: left 407168 vs. right 993 copies/100 ng DNA, $P < 0.05$, Mann-Whitney *U* test, Fig. 4). No significant left-right tissue difference in VZ+434 levels in DRG samples was observed (Fig. 4), suggesting that plasmid uptake is restricted to the site of injection, resulting in upregulation of VEGF-A in the muscle, consistent with previous observations (27). Importantly, the results demonstrate that axonal transport of VZ+434 plasmid is not responsible for the increased VEGF-A levels in the DRG.

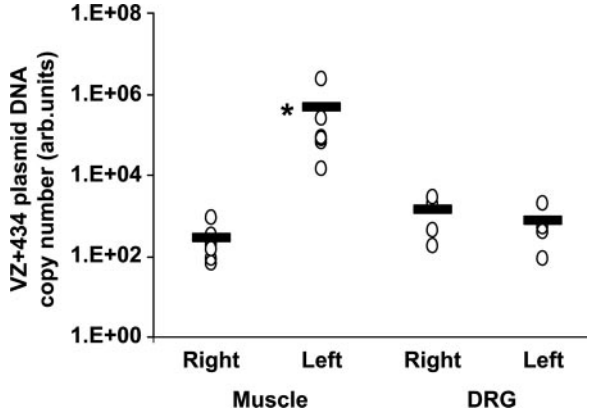

FIG. 4. Expression of VZ+434 DNA plasmid copy number in ipsilateral and contralateral tissues. At 24 h after unilateral intramuscular injection of VZ+434 (250 μg), tissues were harvested and DNA was extracted. The background PCN of VZ+434 was set at 2,700 (derived from mean + 2 SD from contralateral tissue samples). Data from individual animals are shown as circles, with the mean as a horizontal bar ($n = 8$ for muscle and $n = 4$ for DRG). Ipsilateral muscle contained significantly more copies of VZ+434 per 100 ng DNA than contralateral muscle, whereas there was no significant left-right tissue difference in VZ+434 in DRG (*$P < 0.05$, Mann-Whitney *U* test).

VEGF-A undergoes axonal transport in sciatic nerve in vivo. Axonal transport of VEGF-A protein in the sciatic nerve of diabetic rats was assessed using immunocytochemistry and Western blotting techniques (Fig. 5). Ligation of the sciatic nerve of diabetic rats injected distally with VZ+434 caused an increase in VEGF-A-IR both proximal and, notably, distal to the ligature site (Fig. 5*A*). VEGF-A-IR was clearly observed in axonal profiles; a region is highlighted and shown as inset (Fig. 5*A* and *B*, arrows). VEGF-A-IR did not colocalize with S100-IR Schwann cells (Fig. 5*C*).

Ligation of the sciatic nerve of untreated diabetic rats showed very little axonal accumulation of VEGF-A-IR (Fig. 5*E*), restricted to the regions of nerve immediately adjacent to the ligature, a marked contrast to the wide distribution of VEGF-A-IR in the VZ+434-injected rats, particularly throughout the distal nerve (Fig. 5*A*, arrows). VEGF-A-IR was absent from the contralateral nerve (Fig. 5*D*).

Ligation of the sciatic nerve of control rats (nondiabetic), either injected with VZ+434 (Fig. 5*G*) or left untreated (Fig. 5*F*), revealed an accumulation of VEGF-A-IR proximal and distal to the ligature site.

These observations were confirmed by Western blot analysis of VEGF-A protein levels in nerve segments taken proximal and distal to the ligature (schematic diagram illustrated in Fig. 5*H*). Protein levels were quantified by densitometric analysis. Increased VEGF-A was observed particularly in all distal segments and segments immediately proximal to the ligature site in diabetic rats injected with VZ+434 (Fig. 5*I*). In contrast, sciatic nerve samples prepared from control rats injected with VZ+434 showed a more even distribution of VEGF-A throughout the whole nerve (Fig. 5*J*), with the greatest accumulation observed in the proximal segment adjacent to the ligature (Fig. 5*J*). Together these data demonstrate that VEGF-A undergoes axonal transport to the DRG and that intramuscular administration of VZ+434 is sufficient to overcome the deficit in VEGF-A levels observed in this tissue in this STZ model of diabetes.

Ligation of the sciatic nerve reduced the VZ+434-mediated increase in VEGF-A in the DRG. Diabetes was associated with a significant decrease in basal VEGF-A protein levels in the DRG (Fig. 1*B* and supplementary Fig. 1*A* and *B*, available in an online appendix at http://diabetes.diabetesjournals.org/cgi/content/full/db08-1526/DC1), and VZ+434 administration restored VEGF-A to control levels (supplementary Fig. 1*A* and *B*). However, this increase was markedly reduced by ligation of the sciatic nerve in three of five animals tested (mean change across all five animals was not significant) (supplementary Fig. 1*A* and *B*). Taken together with the absence of plasmid DNA encoding VZ+434 in the DRG, these data suggest that the observed normalization of VEGF-A levels in the DRG after VZ+434 treatment occurs via retrograde axonal transport of VEGF-A protein in the sciatic nerve.

VEGF-A accumulation in the DRG is associated with activation of the PI3-K pathway. To analyze the functional consequences of elevated VEGF-A levels in the DRG, we investigated intracellular signaling pathways potentially responsible for the VEGF-A–mediated neuroprotective effects in diabetic neuropathy. Specifically, we investigated activation of p38 MAPK, ERK1/2, and PI3-K pathways using phospho-specific antibodies. Neither the levels nor the phosphorylation status of the MAPKs p38 and ERK1/2 was significantly altered in the DRG of VZ+434-injected diabetic rats at any time point studied

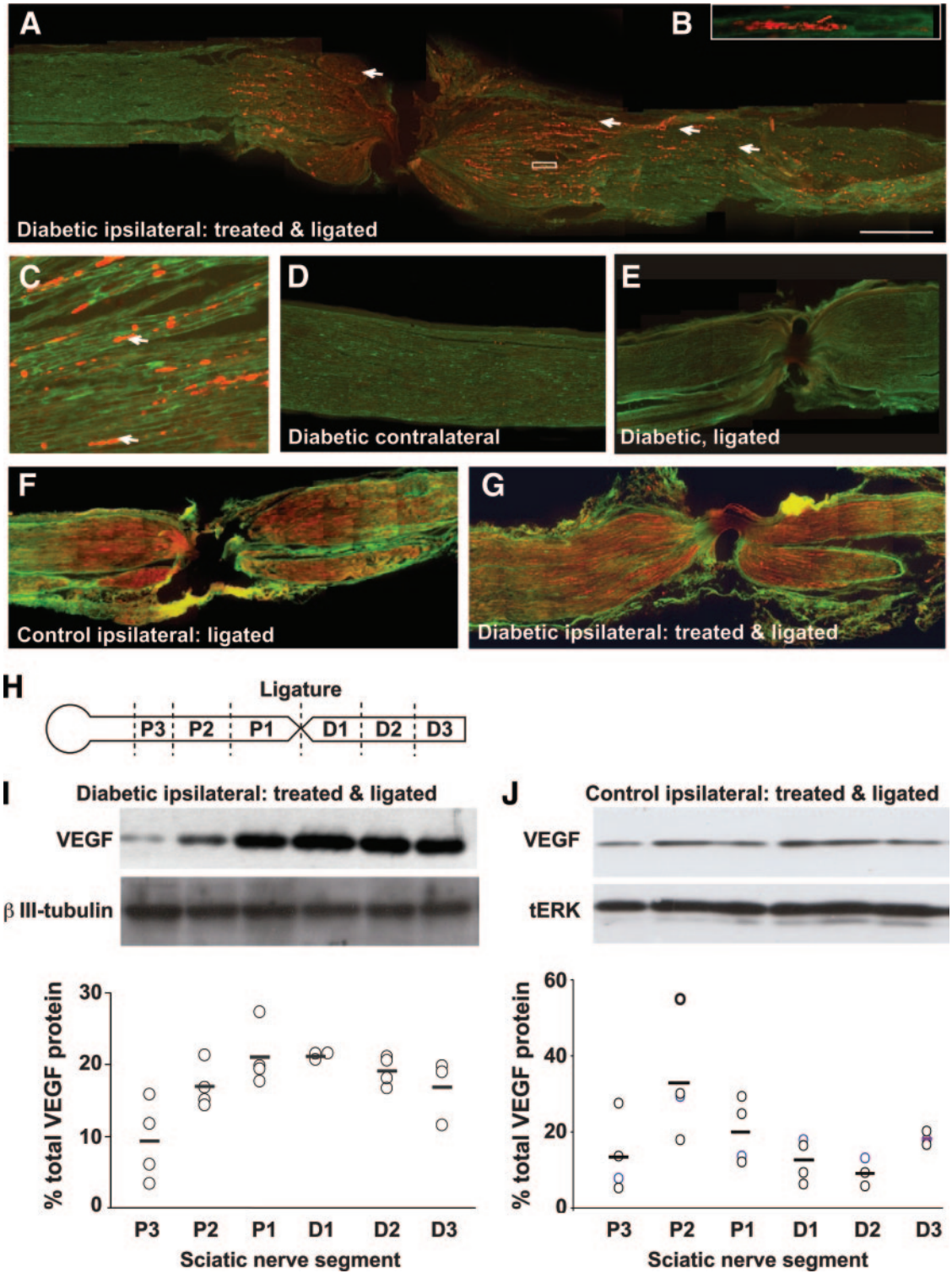

FIG. 5. VEGF-A undergoes axonal transport in the sciatic nerve in vivo. Adult rats received a unilateral sciatic nerve ligature at mid-thigh level, proximal to the site of VZ+434 injection (250 μg, intramuscularly) Longitudinal sections of sciatic nerve, 24 h after ligation, were immunostained for VEGF-A (red) and S100 to label Schwann cells (green; *A–G*). VEGF-A-IR can clearly be seen to accumulate within axons (*A*, arrows) at the ligature site, proximal and distal to the ligature site, indicating bidirectional axonal transport. A region highlighted by a rectangle in (*A*) is shown at increased magnification in (*B*). VEGF-A-IR was restricted to axons and not Schwann cells (*B* and *C*). Little VEGF-A-IR was observed in unligated contralateral nerve (*D*) or untreated ligated nerve (*E*). In contrast, VEGF-IR accumulated both proximal and distal to ligatures in both untreated (*F*) or treated (*G*) control rats. Scale bars = 1 mm. Ligated sciatic nerves from VZ+434-injected STZ-induced diabetic rats (*I*) or control rats (*J*) were cut into 5-mm segments proximal and distal to the ligature and samples processed for Western blotting to assess VEGF-A levels (see schematic diagram, *H*). VEGF-A accumulated both proximal and particularly distal to the ligature in VZ+434-injected diabetic rats (*I*). Samples prepared from control rats injected with VZ+434 showed the greatest accumulation of VEGF in proximal samples (*J*). Data for individual animals are shown as circles; the mean value is shown as a horizontal bar (*I* and *J*). (A high-quality digital representation of this figure is available in the online issue.)

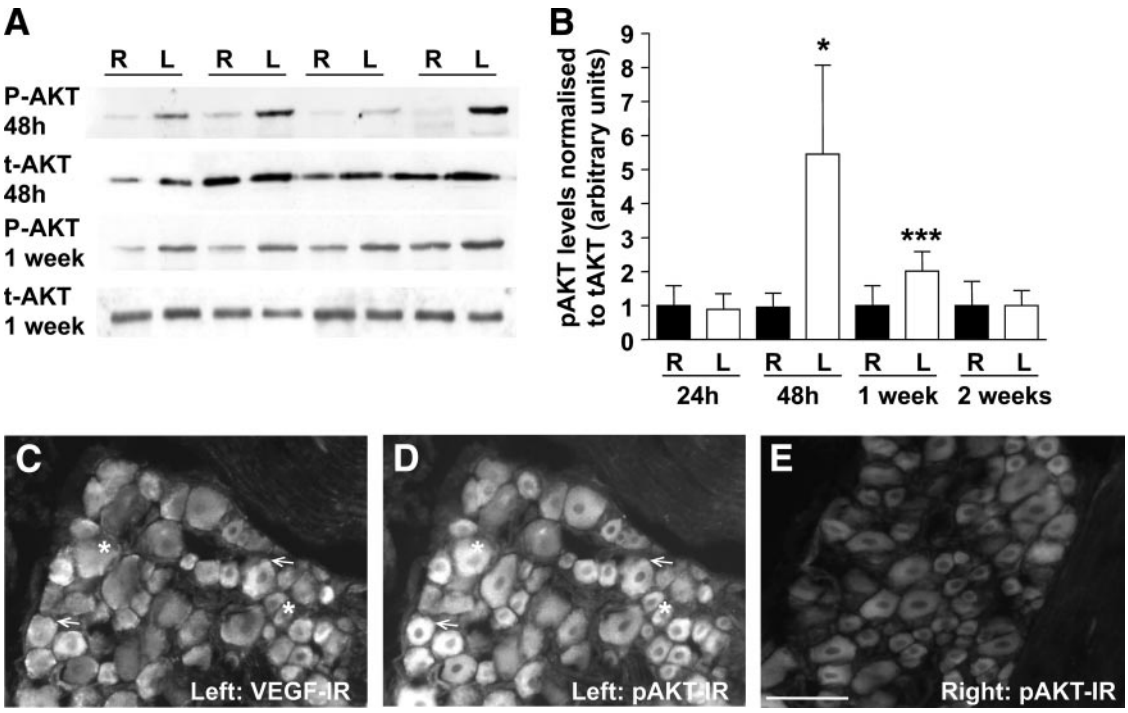

FIG. 6. AKT is phosphorylated in ipsilateral L4/5 DRG after VZ+434 injection. Diabetic rats (3 weeks after STZ injection) treated with VZ+434 were killed at the indicated time points after injection (24 h, 48 h, 1 week, 2 weeks; $n = 4$ per time point). Phosphorylated (p-AKT) and total (t-AKT) AKT levels in right (uninjected, contralateral limb) and left (injected, ipsilateral limb) DRG were assessed using Western blotting (*A*) and quantified using densitometry (*B*). Intramuscular administration of VZ+434 caused a rapid and significant ipsilateral increase in pAKT levels in L4/5 DRG (*A* and *B*) by 48 h after injection ($*P < 0.05$) and remained significantly elevated for 1 week ($***P < 0.001$). Immunocytochemical analysis with antibodies against VEGF-A and pAKT showed colabeling of VEGF-A-IR (*C*) and pAKT (*D*) neurons in the DRG (arrows), however, pAKT-IR neurons that did not colocalize with VEGF-IR neurons were also observed (asterisk). Reduced pAKT-IR was observed in contralateral DRG (*E*). Scale bar, 50 μm.

(e.g., 24 h after injection: p38: ipsilateral 1.2 ± 0.51 versus contralateral 1.0 ± 0.73 AU, $P > 0.05$, $n = 4$; ERK1/2: ipsilateral 1.56 ± 0.25 versus contralateral 1.0 ± 0.34 AU, $P > 0.05$, $n = 4$).

In contrast, an increase in AKT phosphorylation was observed in the ipsilateral L4/5 DRG 48 h after VZ+434 injection (left: 5.4 ± 2.6 versus right: 1.0 ± 0.4 AU, $P < 0.05$, $n = 4$), and activation was maintained for 1 week (left: 2.0 ± 0.6 versus right: 1.0 ± 0.6 AU, $P < 0.01$, $n = 4$; Fig. 6*A* and *B*). This increase in pAKT in the ipsilateral compared with contralateral DRG was confirmed using immunocytochemical analysis (Fig. 6*C–F*). Ipsilateral and contralateral DRG were colabeled with antibodies against VEGF-A (Fig. 6*C* and *E*) and pAKT (Fig. 6*D* and *F*). A threefold increase in neurons expressing pAKT-IR was observed in the ipsilateral DRG compared with the contralateral DRG (Fig. 6*D* and *F* arrows; left: 10% pAKT-IR neurons versus right 3% pAKT-IR neurons, $P < 0.05$). Furthermore, of the pAKT-IR neurons 61% coexpressed VEGF-IR and of the VEGF-IR neurons 85% coexpressed pAKT-IR. Because pAKT-IR is observed in a greater number of neurons than those possessing VEGF-IR, this may suggest a paracrine action of VZ+434-generated and -transported VEGF-A within the DRG.

Intramuscular administration of VZ+434 protects against mechanical allodynia. To determine whether the VZ+434-mediated increase of VEGF-A in small- to medium-diameter neurons has protective effects in experimental diabetic neuropathy, we investigated the functional efficacy of VZ+434 on the development of mechanical hypersensitivity and/or hyposensitivity in STZ-induced diabetic rats (Fig. 7).

Eight weeks after the induction of diabetes, hind paw thresholds to mechanical stimulation were significantly reduced compared with pre-STZ thresholds (Fig. 7*A*) and age-matched control rats (Fig. 7*B*). Similarly, paw withdrawal response thresholds from the contralateral hind limb of STZ-induced diabetic rats treated with VZ+434 were reduced compared with both pre-STZ values (Fig. 7*A*) and age-matched control rats (Fig. 7*C*). However, VZ+434 treatments provided significant protection against mechanical allodynia in the left hind paw 8 weeks after STZ injection (Fig. 7*A* and *D*). This suggests that the VZ+434-mediated increase of VEGF-A in the DRG protects against the mechanical hypersensitivity observed in STZ-induced diabetes.

DISCUSSION

This study demonstrates that VEGF-A protein levels in the DRG are reduced in STZ-induced diabetic rats at early stages of the disease (3 weeks after STZ injection). This deficit was corrected by intramuscular administration of VZ+434, a plasmid that encodes a zinc finger protein-transcription factor capable of simulating endogenous production of VEGF-A. There was no evidence of VZ+434 plasmid DNA being transported to, or transcribed within, the DRG, rather VEGF-A protein was axonally transported to sensory neurons in ipsilateral L4/5 DRG 24 h after injection, and was associated with altered signal transduction, via the PI3-K pathway. Treatment with VZ+434 provided unilateral protection against mechanical allodynia 8 weeks after STZ injection.

VEGF-A was localized to small- to medium-diameter

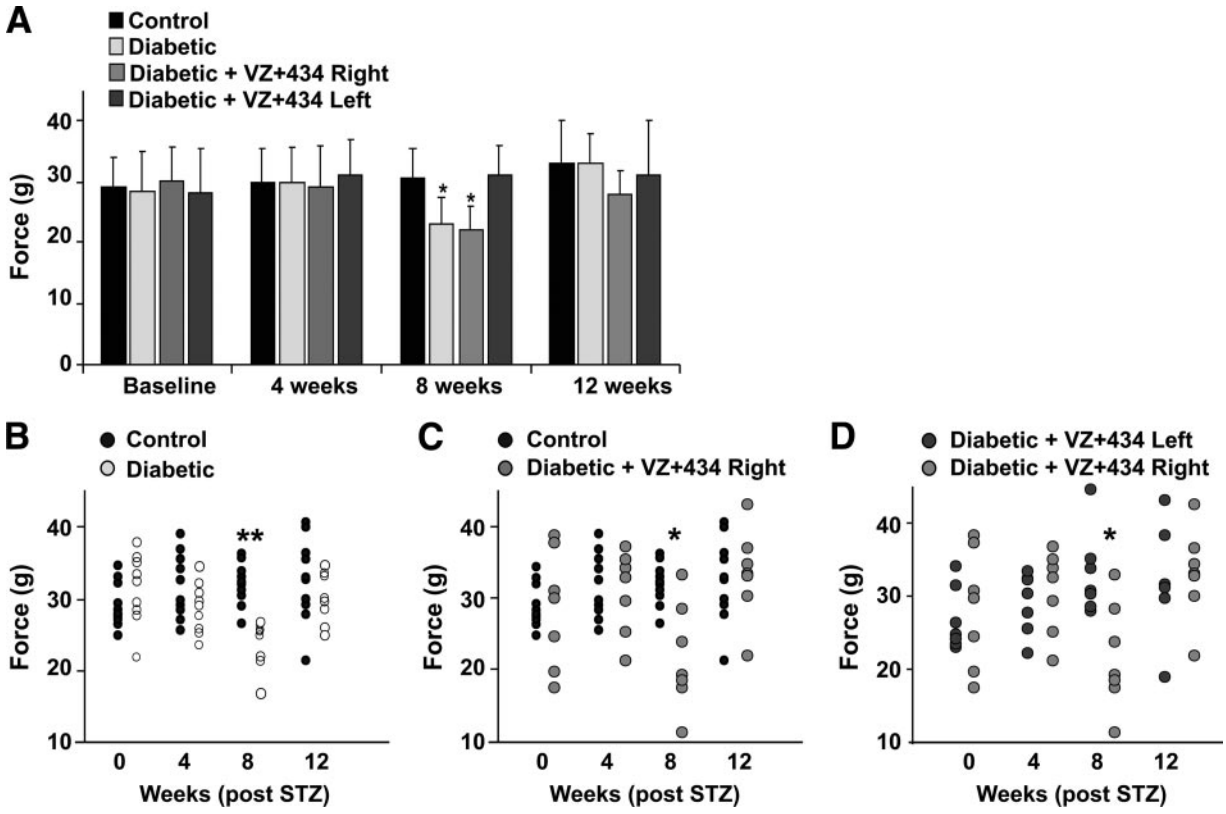

FIG. 7. VZ+434 protects against mechanical hyperalgesia. Sensory testing was conducted prior to treatment (baseline measures) and at 4, 8, and 12 weeks after STZ injection. VZ+434-treated rats received unilateral intramuscular injections at 4, 6, and 8 weeks after STZ injection. At the 4- and 8-week time points, mechanical thresholds were assessed 3 days after VZ+434. At 8 weeks after STZ injection, a significant decrease in the paw withdrawal force (PWF) was observed in STZ-induced diabetic rats and in the contralateral hind paw of VZ+434-treated STZ-induced diabetic rats compared with their baseline measures (*A*, mean + SD, **P* < 0.05, *n* = 7–9, two-way ANOVA, Bonferroni multiple comparison test). At 8 weeks, STZ-induced diabetic rats (*B*) and the contralateral hind paw of VZ+434-treated rats (*C*) compared with nondiabetic controls (*B* and *C*). VZ+434 treatment (*D*) provided significant protection against this allodynia in the ipsilateral limb (*B–D*, data shown for individual animals **P* < 0.05; ***P* < 0.01, *n* = 7–9, one-way ANOVA, Dunnett post hoc test).

sensory neurons in the DRG of control rats, confirming previous studies (2,5), and was downregulated 3 weeks after induction of diabetes. The time course of VEGF-A expression in the DRG after induction of diabetes has not been systematically characterized to date, and evidence suggests a dynamic regulation over the course of the disease. VEGF-A-IR has been reported to be upregulated in the DRG 12 weeks after STZ injection in mice (28), however we found no change in VEGF-A protein levels 12 weeks after STZ injection in rats (data not shown).

Receptors for VEGF-A have previously been characterized in sensory neurons (8,9,29). Neurons appear to lack VEGFR-1, which is largely expressed by endothelial cells (30,31). Conflicting evidence exists about the neuronal expression of VEGFR-2 in sensory neurons. Sondell et al. (2,5,6) describe a postnatal decrease in the percentage of VEGFR-2-IR neurons in the DRG, with less than 10% of sensory neurons expressing VEGFR-2 in adult mouse DRG. These VEGFR-2–positive neurons were of the large-diameter RT97-positive population and the small-diameter CGRP-IR population; no IB4-positive neurons expressed VEGFR-2 (6). In contrast, other groups did not detect VEGFR-2 in sensory neurons (31). Neuropilin-1 is highly expressed in sensory neurons (6,31,32); however, the neuropilin receptors lack defined signaling motifs and appear to act as a coreceptor for VEGFR-2.

A decrease in VEGF-A in sensory neurons may be a functional defect associated with the pathogenesis of diabetic neuropathy. Indeed, clinical studies by Quattrini et al. identified a significant reduction in VEGF-A levels and endothelial cell dysfunction, and a loss in intraepidermal nerve fibers, in skin biopsy samples taken from patients with increasing severity of diabetic neuropathy (33). Diabetic neuropathy is a heterogeneous disease with a widely varying pathology including a neurotrophin deficit. A deficit in nerve growth factor (NGF) expression by sensory neuron targets and retrograde transport to the DRG is well established in experimental diabetic neuropathy (34–36). Indeed, the reduced availability of NGF in experimental diabetic neuropathy provided the rationale of NGF administration as a potential treatment for the disease, and normalizes key molecular and functional aspects of the neuropathy (37,38). It has not been established whether glial cell–derived neurotrophic factor production is similarly impaired in diabetes, however therapy with exogenous glial cell–derived neurotrophic factor in experimental diabetes normalized cutaneous innervation in STZ-induced diabetic mice (39,40). VEGF-A has demonstrated neurotrophic functions in both central and peripheral neurons (4–6), and a number of studies have demonstrated a neuroprotective role for VEGF-A in experimental diabetic neuropathy after administration of VEGF-A by gene transfer (16,17,24). Due to the paradox surrounding VEGF-A in relation to both macrovascular and microvascular complications in diabetes, targeted local delivery of VEGF-A is crucial for the treatment of diabetic neuropathy.

We have previously demonstrated that unilateral intra-

muscular injection of VZ+434 prevents the sensory and motor NCV deficits in the ipsilateral sciatic nerve of STZ-induced diabetic rats (24), and suggested a direct neuroprotective role of VEGF-A in experimental diabetic neuropathy. In this current study, we extend these observations to demonstrate a further neuroprotective effect of VZ+434, namely protection against mechanical allodynia. After intramuscular VZ+434 there is a correction in retrograde axonal transport of VEGF-A in the sciatic nerve to the DRG. As with the NCV change, this effect was restricted to the neurons ipsilateral to the injection. We also observed accumulation of VEGF-A proximal to the ligature, in accordance with other studies showing VEGF axonal transport to be bidirectional (6,16,41).

The mechanism of uptake of VEGF-A by sensory afferent terminals present in the gastrocnemius muscle is unclear. NGF release from cultured smooth muscle cells is elevated in the presence of contractile stimuli (42). It is feasible that, in our study, VEGF-A release from the injected skeletal muscle occurs in this way, aided by the everyday movement of the rats. We postulate that VEGF-A uptake occurs via binding to VEGFR-2; it is well established that upon ligand binding VEGFR-2 is internalized with caveolin-1 and dynamin-2 and undergoes intracellular trafficking and nuclear localization, via microtubules and the endocytic pathway (43–47).

VZ+434-induced VEGF-A activates the cytoplasmic Ser/Thr kinase AKT in L4/5 DRG ipsilateral to the VZ+434 injection. The downstream targets of VEGF-A/AKT activation are currently under investigation. The PI3-K pathway is activated by many growth factors including IGFs, insulin, and NT-3 in sensory neurons (48–51), all of which are reduced in diabetic neuropathy (13,52,53). Furthermore, VEGF-A increases pAKT in primary cultures of dissociated rat sensory neurons (data not shown). A study using the PI3-K inhibitor, LY294002, on mice DRG explants implicated this pathway in sensory neuron survival, as LY294002 caused a dose-dependent cell death (54). PI3-K promotes neuronal cell survival by modulation of Bcl-2 and thus mitochondria function, and regulates energy metabolism in sensory neurons. In addition, activation of the PI3-K/AKT pathway increases axonal caliber and terminal branching of sensory neurons in vitro (55) and thus plays an important role in axon morphological differentiation.

Because phosphorylation of AKT occurs in a greater number of neurons than those possessing VEGF-A-IR after VZ+434 administration, this may support the notion of both an autocrine and paracrine action of transported VEGF-A within the DRG. This could also explain how expression of VEGF-A, by small- to medium-diameter neurons in the DRG, may ameliorate the NCV deficits measured in large-diameter myelinated axons in diabetic neuropathy (24), as increased pAKT-IR is observed in all populations of sensory neurons, however further experiments would be necessary to confirm this. Alternatively, NCV deficits may be ameliorated by another, as yet unidentified, mechanism such as restoration of nerve blood flow.

Our current work suggests that VEGF-A is able to modulate the PI3-K signaling cascade in the L4/5 DRG, which may underlie the neuroprotective action of VZ+434 in the management of diabetic neuropathy.

ACKNOWLEDGMENTS

E.J.P. and B.D.-J. were supported by the Medical Research Council (U.K.) and the University of Manchester. N.J.G. was supported by Research Council UK and British Pharmacological Society (U.K.).

S.K.S. and R.S. are paid employees of Sangamo BioSciences. S.K.S. is Director of Preclinical Development and receives company incentive stock options and has been involved in the research and development of reagents described in the article. No other potential conflicts of interest relevant to this article were reported.

We thank Sangamo Biosciences, Inc., for the VZ+434 plasmid DNA and study support and Philip Gregory and Steve Zhang for review and helpful comments on the article.

REFERENCES

1. Ferrara N, Gerber HP, LeCouter J. The biology of VEGF and its receptors. Nat Med 2003;9:669–676
2. Sondell M, Kanje M. Postnatal expression of VEGF and its receptor flk-1 in peripheral ganglia. NeuroReport 2001;12:105–108
3. Sondell M, Lundborg G, Kanje M. Regeneration of the rat sciatic nerve into allografts made acellular through chemical extraction. Brain Res 1998;795:44–54
4. Sondell M, Lundborg G, Kanje M. Vascular endothelial growth factor stimulates Schwann cell invasion and neovascularization of acellular nerve grafts. Brain Res 1999;846:219–228
5. Sondell M, Lundborg G, Kanje M. Vascular endothelial growth factor has neurotrophic activity and stimulates axonal outgrowth, enhancing cell survival and Schwann cell proliferation in the peripheral nervous system. J Neurosci 1999;19:5731–5740
6. Sondell M, Sundler F, Kanje M. Vascular endothelial growth factor is a neurotrophic factor which stimulates axonal outgrowth through the flk-1 receptor. Eur J Neurosci 2000;12:4243–4254
7. Lambrechts D, Storkebaum E, Morimoto M, Del-Favero J, Desmet F, Marklund SL, Wyns S, Thijs V, Andersson J, van Marion I, Al-Chalabi A, Bornes S, Musson R, Hansen V, Beckman L, Adolfsson R, Pall HS, Prats H, Vermeire S, Rutgeerts P, Katayama S, Awata T, Leigh N, Lang-Lazdunski L, Dewerchin M, Shaw C, Moons L, Vlietinck R, Morrison KE, Robberecht W, Van Broeckhoven C, Collen D, Andersen PM, Carmeliet P. VEGF is a modifier of amyotrophic lateral sclerosis in mice and humans and protects motoneurons against ischemic death. Nat Genet 2003;34:383–394
8. Ferrara N, Davis-Smyth T. The biology of vascular endothelial growth factor. Endocr Rev 1997;18:4–25
9. Larrivée B, Karsan A. Signaling pathways induced by vascular endothelial growth factor (review). Int J Mol Med 2000;5:447–456
10. Robinson CJ, Stringer SE. The splice variants of vascular endothelial growth factor (VEGF) and their receptors. J Cell Sci 2001;114:853–865
11. Rosenstein JM, Krum JM. New roles for VEGF in nervous tissue: beyond blood vessels. Exp Neurol 2004;187:246–253
12. Fernyhough P, Huang TJ, Verkhratsky A. Mechanism of mitochondrial dysfunction in diabetic sensory neuropathy. J Peripher Nerv Syst 2003;8:227–235
13. Huang TJ, Sayers NM, Verkhratsky A, Fernyhough P. Neurotrophin-3 prevents mitochondrial dysfunction in sensory neurons of streptozotocin-diabetic rats. Exp Neurol 2005;194:279–283
14. Price SA, Agthong S, Middlemas AB, Tomlinson DR. Mitogen-activated protein kinase p38 mediates reduced nerve conduction velocity in experimental diabetic neuropathy: interactions with aldose reductase. Diabetes 2004;53:1851–1856
15. Purves T, Middlemas A, Agthong S, Jude EB, Boulton AJ, Fernyhough P, Tomlinson DR. A role for mitogen-activated protein kinases in the etiology of diabetic neuropathy. FASEB J 2001;15:2508–2514
16. Chattopadhyay M, Krisky D, Wolfe D, Glorioso JC, Mata M, Fink DJ. HSV-mediated gene transfer of vascular endothelial growth factor to dorsal root ganglia prevents diabetic neuropathy. Gene Ther 2005;12:1377–1384
17. Schratzberger P, Walter DH, Rittig K, Bahlmann FH, Pola R, Curry C, Silver M, Krainin JG, Weinberg DH, Ropper AH, Isner JM. Reversal of experimental diabetic neuropathy by VEGF gene transfer. J Clin Invest 2001;107:1083–1092
18. Simovic D, Isner JM, Ropper AH, Pieczek A, Weinberg DH. Improvement in chronic ischemic neuropathy after intramuscular phVEGF165 gene transfer in patients with critical limb ischemia Arch Neurol 2001;58:761–768

19. Rebar EJ, Huang Y, Hickey R, Nath AK, Meoli D, Nath S, Chen B, Xu L, Liang Y, Jamieson AC, Zhang L, Spratt SK, Case CC, Wolffe A, Giordano FJ. Induction of angiogenesis in a mouse model using engineered transcription factors. Nat Med 2002;12:1427–1432
20. Whitlock PR, Hackett NR, Leopold PL, Rosengart TK, Crystal RG. Adenovirus-mediated transfer of a minigene expressing multiple isoforms of VEGF is more effective at inducing angiogenesis than comparable vectors expressing individual VEGF cDNAs. Mol Ther 2004;9:67–75
21. Yu J, Lei L, Liang Y, Hinh L, Hickey RP, Huang Y, Liu D, Yeh JL, Rebar EJ, Case CC, Spratt SK, Sessa WC, Giordano FJ. An engineered VEGF-activating zinc finger protein transcription factor improves blood flow and limb salvage in advanced-age mice. FASEB J 2006;3:479–481
22. Liu PQ, Rebar EJ, Zhang L, Liu Q, Jamieson AC, Liang Y, Qi H, Li PX, Chen B, Mendel MC, Zhong X, Lee YL, Eisenberg SP, Spratt SK, Case CC, Wolffe AP. Regulation of an endogenous locus using a panel of designed zinc finger proteins targeted to accessible chromatin regions: activation of vascular endothelial growth factor A. J Biol Chem 2001;276:11323–11334
23. Dai Q, Huang J, Klitzman B, Dong C, Goldschmidt-Clermont PJ, March KL, Rokovich J, Johnstone B, Rebar EJ, Spratt SK, Case CC, Kontos CD, Annex BH. Engineered zinc finger-activating vascular endothelial growth factor transcription factor plasmid DNA induces therapeutic angiogenesis in rabbits with hindlimb ischemia. Circulation 2004;110:2467–2475
24. Price SA, Dent C, Duran-Jimenez B, Liang Y, Zhang L, Rebar EJ, Case CC, Gregory PD, Martin TJ, Spratt SK, Tomlinson DR. Gene transfer of an engineered transcription factor promoting expression of VEGF-A protects against experimental diabetic neuropathy. Diabetes 2006;55:1847–1854
25. Karamoysoyli E, Burnand RC, Tomlinson DR, Gardiner NJ. Neuritin mediates nerve growth factor-induced axonal regeneration and is deficient in experimental diabetic neuropathy. Diabetes 2008;57:181–189
26. Rose RD, Rohrlich D. Counting sectioned cells via mathematical reconstruction. J Comp Neurol 1988;272:365–386
27. Xie D, Li Y, Reed EA, Odronic SI, Kontos CD, Annex BH. An engineered vascular endothelial growth factor-activating transcription factor induces therapeutic angiogenesis in ApoE knockout mice with hindlimb ischemia. J Vasc Surg 2006;44:166–175
28. Samii A, Unger J, Lange W. Vascular endothelial growth factor expression in peripheral nerves and dorsal root ganglia in diabetic neuropathy in rats. Neurosci Lett 1999;262:159–162
29. Carmeliet P, Ferreira V, Breier G, Pollefeyt S, Kieckens L, Gertsenstein M, Fahrig M, Vandenhoeck A, Harpal K, Eberhardt C, Declercq C, Pawling J, Moons L, Collen D, Risau W, Nagy A. Abnormal blood vessel development and lethality in embryos lacking a single VEGF allele. Nature 1996;380:435–439
30. Cheng L, Jia H, Löhr M, Bagherzadeh A, Holmes DI, Selwood D, Zachary I. Anti-chemorepulsive effects of vascular endothelial factor and placental growth factor-2 in dorsal root ganglion neurons are mediated via neuropilin-1 and cyclooxygenase-derived prostanoid production. J Biol Chem 2004;279:30654–30661
31. Kutcher ME, Klagsbrun M, Mamluk R. VEGF is required for the maintenance of dorsal root ganglia blood vessels but not neurons during development. FASEB J 2004;18:1952–1954
32. Gavazzi I, Kumar RD, McMahon SB, Cohen J. Growth responses of different subpopulations of adult sensory neurons to neurotrophic factors in vitro. Eur J Neurosci 1999;11:3405–3414
33. Quattrini C, Jeziorska M, Boulton AJ, Malik RA. Reduced vascular endothelial growth factor expression and intra-epidermal nerve fiber loss in human diabetic neuropathy. Diabetes Care 2008;31:140–145
34. Fernyhough P, Diemel LT, Hardy J, Brewster WJ, Mohiuddin L, Tomlinson DR. Human recombinant nerve growth factor replaces deficient neurotrophic support in the diabetic rat. Eur J Neurosci 1995;7:1107–1110
35. Hellweg R, Hartung HD. Endogenous levels of NGF are altered in experimental diabetes mellitus: a possible role for NGF in the pathogenesis of diabetic neuropathy. J Nerosci Res 1990;26:258–267
36. Hellweg R, Raivich G, Hartung H-D, Hock C, Kreutzberg GW. Axonal transport of endogenous nerve growth factor (NGF) and NGF receptor in experimental diabetic neuropathy. Exp Neurol 1994;130:24–30
37. Fernyhough P, Diemel LT, Brewster WJ, Tomlinson DR. Altered neurotrophin mRNA in peripheral nerve and skeletal muscle of experimentally diabetic rats. J Neurochem 1995;64:1231–1237
38. Apfel SC, Arezzo JC, Brownlee M, Federoff H, Kessler JA. Nerve growth factor administration protects against experimental diabetic sensory neuropathy. Brain Res 1994;634:7–12
39. Christianson JA, Riekhof JT, Wright DE. Restorative effects of neurotrophin treatment on diabetes-induced cutaneous axon loss in mice. Exp Neurol 2003;179:188–199
40. Christianson JA, Ryals JM, Johnson MS, Dobrowsky RT, Wright DE. Neurotrophic modulation of myelinated cutaneous innervation and mechanical sensory loss in diabetic mice. Neuroscience 2007;145:303–313
41. Storkebaum E, Lambrechts D, Dewerchin M, Moreno-Murciano MP, Appelmans S, Oh H, Van Damme P, Rutten B, Man WY, De Mol M, Wyns S, Manka D, Vermeulen K, Van Den Bosch L, Mertens N, Schmitz C, Robberecht W, Conway EM, Collen D, Moons L, Carmeliet P. Treatment of motoneuron degeneration by intracerebroventricular delivery of VEGF in a rat model of ALS. Nat Neurosci 2004;8:85–92
42. Tuttle JB, Etheridge R, Creedon DJ. Receptor-mediated stimulation and inhibition of nerve growth factor secretion by vascular smooth muscle. Exp Cell Res 1993;208:350–361
43. Labrecque L, Royal I, Surprenant DS, Patterson C, Gingras D, Béliveau R. Regulation of vascular endothelial growth factor receptor-2 activity by caveolin-1 and plasma membrane cholesterol. Mol Biol Cell 2003;14:334–347
44. Li W, Keller G. VEGF nuclear accumulation correlates with phenotypical changes in endothelial cells. J Cell Sci 2000;113:1525–1534
45. Meyer RD, Dayanir V, Majnoun F, Rahimi N. The presence of a single tyrosine residue at the carboxyl domain of vascular endothelial growth factor receptor-2/FLK-1 regulates its autophosphorylation and activation of signaling molecules. J Biol Chem 2002;277:27081–27087
46. Bhattacharya R, Kang-Decker N, Hughes DA, Mukherjee P, Shah V, McNiven MA, Mukhopadhyay D. Regulatory role of dynamin-2 in VEGFR-2/KDR-mediated endothelial signaling. FASEB J 2005;19:1692–1694
47. Mitola S, Brenchio B, Piccinini M, Tertoolen L, Zammataro L, Breier G, Rinaudo MT, den Hertog J, Arese M, Bussolino F. Type I collagen limits VEGFR-2 signaling by a SHP2 protein-tyrosine phosphatase-dependent mechanism 1. Circ Res 2006;98:45–54
48. Brunet A, Datta SR, Greenberg ME. Transcription-dependent and -independent control of neuronal survival by the PI3K-Akt signaling pathway. Curr Opin Neurobiol 2001;11:297–305
49. Dudek H, Datta SR, Franke TF, Birnbaum MJ, Yao R, Cooper GM, Segal RA, Kaplan DR, Greenberg ME. Regulation of neuronal survival by the serine-threonine protein kinase Akt. Science 1997;275:661–665
50. Orike N, Middleton G, Borthwick E, Buchman V, Cowen T, Davies AM. Role of PI 3-kinase, Akt and Bcl-2-related proteins in sustaining the survival of neurotrophic factor-independent adult sympathetic neurons. J Cell Biol 2001;154:995–1005
51. Orike N, Thrasivoulou C, Wrigley A, Cowen T. Differential regulation of survival and growth in adult sympathetic neurons: an in vitro study of neurotrophin responsiveness. J Neurobiol 2001;47:295–305
52. Feldman EL, Russell JW, Sullivan KA, Golovoy D. New insights into the pathogenesis of diabetic neuropathy. Curr Opin Neurol 1999;12:553–563
53. Middlemas A, Delcroix JD, Sayers NM, Tomlinson DR, Fernyhough P. Enhanced activation of axonally transported stress-activated protein kinases in peripheral nerve in diabetic neuropathy is prevented by neurotrophin-3. Brain 2003;126:1671–1682
54. Edström A, Ekström PA. Role of phosphatidylinositol 3-kinase in neuronal survival and axonal outgrowth of adult mouse dorsal root ganglia explants. J Neurosci Res 2003;75:726–735
55. Markus A, Zhong J, Snider WD. Raf and akt mediate distinct aspects of sensory axon growth. Neuron 2002;35:65–76